scientific reports

Check for updates

OPEN

Cutaneous wound healing functions of novel milk-derived antimicrobial peptides, hLFT-68 and hLFT-309 from human lactotransferrin, and bLGB-111 from bovine *β*-lactoglobulin

Xixian Li[1,2,3], Wanning Zhang[1,2,3], Wenhao Yu[2], Yang Yu[2], Huiyuan Cheng[2], Yuyang Lin[1], Jingwen Feng[2], Muxin Zhao[1]✉ & Yan Jin[2]✉

The absence of multi-functional antimicrobial agents in clinical settings hinders cutaneous wound healing. Milk-derived antimicrobial peptides (MAPs) may be the imperative solution to wound repair, combining the dermatic curative properties of antimicrobial peptides with the biological activity of milk. Three novel MAPs, which were hLFT-68 (IAENRADAV) and hLFT-309 (GSPSGQKDLLF) identified in human milk and bLGB-111 (LDTDYKKY) identified in bovine milk in our previous work, were initially investigated for their function in wound healing. In vitro, the antibacterial activity and cellular mechanism of the MAPs were examined. It was found that they presented inhibition for *Staphylococcus aureus* and *Escherichia coli*, decreased the secretion of inflammatory factors (IL-1*β*, IL-6, and TNF-*α*), and promoted fibroblast and keratinocyte proliferation. An infected wound model was established to evaluate the in vivo anti-inflammatory and regeneration properties of the MAPs. The wound area shrank more rapidly, and the wound inflammation was reduced by MAP treatment. Especially on days 3–5 after mouse modeling, the wound repair rate increased by up to 35%. Furthermore, it was suggested that they encouraged collagen synthesis and deposition, and tissue regeneration. The presented results indicated that MAPs accelerated the recovery of infected wounds, possessing the potential for developing wound-healing therapy.

Keywords Milk-derived peptide, Antimicrobial peptide, Wound healing, Skin regeneration, Anti-inflammatory effect

Abbreviations

ECM	Extracellular matrix
EGF	Epidermal growth factor
EGFR	Epidermal growth factor receptor
FGF	Fibroblast growth factor
hBD	Human beta-defensin
HSF	Human skin fibroblasts
IL	Interleukin
IOD	Integrated optical density
LPS	Lipopolysaccharide
MAP	Milk-derived antimicrobial peptides

[1]Department of Plastic Surgery, The Second Affiliated Hospital of Dalian Medical University, No.467, Zhongshan Road, Dalian 116023, Liaoning, China. [2]CAS Key Laboratory of Separation Science for Analytical Chemistry, Dalian Institute of Chemical Physics, Chinese Academy of Sciences, No.457, Zhongshan Road, Dalian 116023, Liaoning, China. [3]Xixian Li and Wanning Zhang contributed equally to this work. ✉email: zhaomuxin@126.com; yanjin@dicp.ac.cn

MAPK	Mitogen-activated protein kinase
MIC	Minimal inhibit concentrations
NF-κB	Nuclear factor-kappa B
TGF	Transforming growth factor
TLR	Toll-like receptor
TNF	Tumor necrosis factor
VAN	Vancomycin
α-SMA	Alpha-smooth muscle actin

Skin is an adaptable, versatile, and outermost organ in the human body, consisting of the dermis and the epidermis, which shields humans from chemical, physical, and ultraviolet radiation threats. These external injuries are deep into the epidermis, dermis, or even subcutaneous tissues causing difficulties in healing wounds[1,2]. Cutaneous wound healing is a collaborative, complex, and multifaceted process with four different and overlapping phases: hemostasis, inflammation, proliferation, and remodeling. (1) During the hemostasis phase, damaged cells activate the blood coagulation system, developing clots to stop bleeding and protect the injured site from infection. (2) During the inflammation phase, neutrophils clean cellular debris and kill the pathogen, while monocytes transform into macrophages to eliminate any remaining cellular debris. (3) During the proliferation phase, keratinocytes and fibroblasts migrate and proliferate, producing collagen and depositing extracellular matrix (ECM) components. Vascular endothelial cells initiate the formation of new blood vessels. (4) During the remodeling phase, fibroblasts remodel ECM and differentiate into myofibroblasts[2–5].

To date, it can be tricky for a single conventional medication to meet al.l of the requirements of the four wound-healing phases, and treating chronic wounds can still be challenging. Millions of individuals worldwide are affected by the major clinical issues of wound chronicity and poor healing. The problem becomes worse owing to the drawbacks of conventional wound-healing medications of a single effect, high cost, polypharmacy, and long-term use, which place a significant financial strain on the healthcare system[6,7]. In the treatment of chronic wounds, it is necessary to treat them with umpty medications that promote the proliferation of cutaneous cells, are antibacterial, improve revascularization, increase the local oxygen partial pressure, deactivate the inflammation, enhance the wound microenvironment, and so on[8–10]. Antimicrobial peptides not only protect wounds from microbial infection, but also enhance skin barrier homeostasis, modify inflammatory responses, and accelerate wound healing[11]. Antimicrobial peptide therapies possess the solution to these issues, which might become a potential multifunctional agent or adjuvant in biomedical, pharmaceutical, and cosmeceutical applications[12].

Antimicrobial peptides are produced by multicellular organisms as a formidable defense mechanism against pathogenic microbes[13]. In addition to broad-spectrum antimicrobial activity, antimicrobial peptides have been investigated to exhibit anti-inflammatory, pro-angiogenic, pro-proliferative, pro-migrative, and little drug-resistant activities. The therapeutic scope covers inflammation, cell proliferation, granulation tissue formation, and tissue remodeling in wound-healing phases[4,14–16]. Besides human antimicrobial peptides such as human beta-defensin (hBD) and LL-37, thousands of natural antimicrobial peptides have been identified in a wide range of species, including invertebrates, mammals, microbes, and plants[4]. There is increased interest in peptides of other new origins due to the different defects of existent antimicrobial peptides.

Mammalian milk is a conveniently available source of well-balanced protein and valuable bioactive peptides. These milk-derived bioactive peptides have an extensive spectrum of biological activity, such as antibacterial, antihypertensive, anti-carcinogenic, antioxidant, antithrombotic, and immunomodulatory properties[17,18]. It has been reported that several milk-derived bioactive peptides promote skin tissue repair and are used in cosmetics and dermatological medications, including glycomacropeptide[19] and VLPVPQK[20].

Antimicrobial peptides from mammalian milk have become a highly effective source[21,22]. Milk-derived antimicrobial peptides (MAPs), among these milk-derived bioactive peptides, are gaining popularity as a safe and effective alternative to antibiotics, with the added benefit of low immunogenicity and low cost, and are applied in food and cosmetic preservation[18,23]. The main known MAPs originate from including α-lactoalbumin, β-lactoglobulin, lactoferrin, and various casein fractions in milk[24]. Through current clinical research, there is promising data indicating lactoferrin may help with psoriasis, acne, and diabetic ulcers, which implies a potential affinity between MAPs and healing wounds[25].

Based on our previous research, three brand-new MAPs, hLFT-68 (IAENRADAV), hLFT-309 (GSPSGQKDLLF), and bLGB-111 (LDTDYKKY), were identified. Through the heat of the protein from human lactoferrin, the hLFT-68 and hLFT-309 were acquired. The bLGB-111 was obtained by enzymatic hydrolysis of the protein from bovine β-lactoglobulin. Considering their plentiful prospective wound-healing advantages, the present study aims to investigate the impact of hLFT-68, hLFT-309, and bLGB-111 on wound repair.

Materials and methods

Synthetic peptides, strains, cell lines and animals

Synpeptide Co., Ltd. (Shanghai, China) was commissioned to synthesize peptides hLFT-68 (IAENRADAV), hLFT-309 (GSPSGQKDLLF), and bLGB-111 (LDTDYKKY) by solid-state method to confirm their purity purities >95%.

E. coli K12 and *S. aureus* were all purchased from the China Center of Industrial Culture Collection (CICC), and preserved in glycerol at − 80 °C. Before the experiment, the two strains were inoculated into liquid Luria-Bertani (LB) broth medium (Sangon Biotech (Shanghai) Co., Ltd., China) and tryptic soy broth (TSB) medium (Shanghai Acmec Biochemical Co., Ltd., China), respectively, and incubated at 37 °C for 12 h to revive, with the process repeated 3 times.

Human skin fibroblasts (HSF), human immortal keratinocytes (HaCaT), and RAW 264.7 cell lines were all purchased from Procell Life Science&Technology Co., Ltd. (Wuhan, China). The cell lines have been checked free of mycoplasma contamination by fluorescent staining. The cell lines were cultured in Dulbecco's modified eagle medium (DMEM, Gibco, Grand Island, NY, USA) supplemented with 10% fetal bovine serum (Gibco, Grand Island, NY, USA), 100 units/mL of penicillin, and 100 units/mL of streptomycin (Gibco, Grand Island, NY, USA) in a humidified 5% CO_2 atmosphere at 37 °C, respectively. All experiments used subconfluent cells (about 80% confluence) grown in a DMEM medium.

Eight-week-old, specific pathogen-free adult male C57BL/6 mice were ordered from Liaoning Changsheng Biotech Co., Ltd. (Liaoning, China) and kept at Dalian Medical University Laboratory Animal Center, Liaoning, China. Experiments were approved and then performed in compliance with the guidelines of the Dalian Institute of Chemical Physics Science Ethics Committee (ethics approval number DICPEC2326). All mice were kept under clean conditions on a 12-hour light/12-hour dark cycle at 22 °C with 75% humidity. Mice were provided with sterilized standard mouse food and water.

Antimicrobial activity assay

The antimicrobial activity of the peptides was evaluated against *E. coli* and *S. aureus*. The minimal inhibit concentrations (MIC, expressed as mg/mL) of hLFT-68, hLFT-309, and hLGB-111 were determined by the broth microdilution method as described in the literature[26,27]. The measurement concentration ranges of hLFT-68, hLFT-309, and hLGB-111 were 102.4, 51.2, 25.6, 12.8, 6.4, 3.2, 1.6, 0.8, 0.4, 0.2, and 0.1 mg/mL. Vancomycin (VAN) was used as the positive control. The MICs were determined as the lowest concentrations of peptide that inhibited visible bacterial growth. The absorbance at 600 nm of each well was measured using a microplate reader (BioTek, VT, USA), and the inhibition rate was calculated by the absorbance. The half maximal inhibitory concentration (IC_{50}, expressed as mg/mL) of hLFT-68, hLFT-309, and hLGB-111 were calculated by inhibition rates and Graphpad Prism version 9.5 software (Graph Software, San Diego, CA, USA)[28].

Inhibition of lipopolysaccharide (LPS)-induced inflammation in vitro

RAW 264.7 cells were used for constructing an LPS-induced inflammatory cell model. Cells were cultured in 96-well plates at a density of 5×10^4 cells/wall overnight. Till cell adherence, the hLFT-68 and hLFT-309 were added per wall in the treatment group to different final concentrations. After 2 h of treatment, LPS (MedChemExpress, NJ, USA) with a final concentration of 1 μg/mL was added to both the treatment and control groups, and the incubation was continued for 24 h[29]. The non-LPS group was set up as a control for model validation. Neither LPS nor other treatments were added to the cells in this group. Then the supernatants were collected and went through centrifugation at 12,000 rpm for 30 min at 4°C. Supernatants were stored at − 80 °C until usage. Tumor necrosis factor (TNF)-α, interleukin (IL)-6, and IL-1β released in the cell-free supernatants from non-stimulated or stimulated culture macrophage cells were measured with enzyme-linked immunosorbent test (ELISA) kits from R&D Systems (Ruixinbio, Quanzhou, China). The ELISA was performed according to the manufacturer's instructions.

Cell proliferation assay

HSF and HaCaT cells were used for the cell proliferation assay by Cell Counting Kit-8 (CCK-8, Seven Biotech, Beijing, China). Cells were added to 96-well plates at a density of 1.5×10^4 cells/wall for 6 h. Then, hLFT-68, hLFT-309, and hLGB-111, respectively, were added per wall to achieve different final peptide concentrations for 24 h. Additionally, human epidermal growth factor (EGF, MedChemExpress, NJ, USA) at final concentrations of 10 μg/mL was added as the positive control. After that, 10 μL of CCK8 solution was added per well, and cells were incubated for a further 1–4 hours. Absorbance at 450 nm was then quantified with a microplate reader. According to the formula below, the cell proliferation rate was calculated:

$$\text{Cell proliferation rate} = \frac{A_{\text{control}} - A_0}{A_x - A_0} \times 100\%$$

where A_0 represents the zero adjusted hole, A_x reflects the absorbance of cells treated with the MAPs, and $A_{control}$ represents the absorbance of cells treated with none of the MAPs. The values of half maximal effective concentration (EC_{50}, expressed as μg/mL) of hLFT-68, hLFT-309, and hLGB-111 were calculated by cell proliferation rates and Graphpad Prism version 9.5 software[30].

Infected full-thickness wound model

Male C57BL/6 mice were used for constructing an infected full-thickness wound model. Mice were injected intraperitoneally with 1% sodium pentobarbital for anesthesia before surgery. After the removal of the dorsal hair, two symmetrical circular full-thickness skin wounds (0.8 cm in diameter) were created on the depilated back skin. Then 50 μL of *S. aureus* at a concentration of 10^7 colony-forming units (CFU)/mL was inoculated into each wound[31]. At the end of each experiment, mice were sacrificed by CO_2 inhalation, which was confirmed by ceasing breath and heartbeat. This model method was used in 2.6. & 2.7. animal experiments.

In vivo study of antimicrobial efficacy

After modeling, mice were randomly assigned to 4 groups (10 mice/group): control, hLFT-68, hLFT-309, and VAN (positive control). The following interventions were performed on both dorsal wounds of mice twice a day: treated with 50μL phosphate buffered solution (PBS, Gibco, Grand Island, NY, USA), 50μL 0.5 mg/mL hLFT-68 group, 50μL 0.5 mg/mL hLFT-309 group, and 50μL 0.15 mg/mL VAN (Bioseth, Zhenjiang, China) as the positive control ($N = 3$) in different groups (PBS as solvent). The intervention was maintained for 4 days. On the

third day following surgery, secretions were collected from the wound site of each group. This was achieved by harvesting and grinding 0.5 g of skin tissue from the wound area. The tissue was harvested using a skin biopsy punch (0.8 cm in diameter), and the excess tissue surrounding the wound was removed until the remaining tissue weighed 0.5 g. The collected secretions were diluted with 5 mL of PBS[32]. 100 µL of the secretion solution was added to the surface of the TSB solid medium for uniform coating and incubated at 37 °C. Photographs of the colonies were taken after 18 h, and the colonies were counted by the Image-Pro Plus 6.0 program.

Quantification of in vivo wound healing

The infected full-thickness wound models shown previously were constructed and group interventions were the same except that the EGF group treated 50 µL of 5000 IU/mL rhEGF (recombinant Human EGF, Kanghesu, Shanghai Haohai Biological Technology Co., Ltd., China) as the positive control ($N=10$). The intervention was maintained for 12 days. The wound area was photographed with a digital camera. The wound repair rate was calculated from the photographs using an image analysis program (Image J, National Institutes of Health; Bethesda, MD, USA) by tracing the wound margin and calculating the pixel area. The measurements were performed in triplicate, and the mean values of consecutive tracings were computed and expressed as a percentage of closure from the original wound. According to the formula below, the wound repair rate was calculated:

$$\text{Wound repair rate} = \left[1 - \left(\frac{S_n}{S_1}\right)\right] \times 100\%$$

where S_n and S_1 are, respectively, the wound area in mice on days n and 1.

At the same time, the inflammation score was recorded every two days. Inflammation score modified and simplified from the Bates-Jensen Wound Assessment Tool[33]: (1) Wound edge: 1 = blurred, unable to distinguish the wound edge; 2 = able to clearly distinguish the wound edge; 3 = clearly distinguishable contour, with the base of the wound lower than the wound edge. (2) Exudate type: 1 = no exudate; 2 = thin light red or pink color exudate; 3 = red or pink color exudate. (3) Exudate volume: 1 = no exudate, wound tissue dry; 2 = wound tissue slightly moist, soaking 0–25% of the dressing; 3 = wound tissue moist, soaking more than 25% of the dressing. (4) Wound color: 1 = normal or pink; 2 = light red; 3 = dark red or purple.

Histological analysis, immunohistochemistry (IHC), and ELISA

Starting on day 0 after surgery, the entire layer of tissue on both sides of the mice's backs was clipped 0.5 cm around the center of the wound at 4-day intervals, which contains the wound and its surrounding normal skin tissue. Skin tissue samples were harvested and fixed with a 4% paraformaldehyde solution (Servicebio, Wuhan, China) for the preparation of histological slides ($N=3$). The slides were subjected to Masson's trichrome staining, as well as Sirius red staining. In addition, the wound tissue slides were also stained by IHC of CD31. All stains and antibodies were purchased from the Servicebio company. Images of stained samples were captured with an optical microscope (Leica, Wetzlar, Germany) or a polarized light microscopy (Leica, Wetzlar, Germany). Collagen volume fraction, collagen types I and III ratio, and mean integrated optical density (IOD) of CD31 were analyzed and calculated from image information of Masson's trichrome staining, sirius red staining, and IHC, respectively, by the Image-Pro Plus 6.0 program (Media Cybernetics, MD, USA).

The biopsy specimens involving the central part of the wounds on days 4, 8, and 12 were obtained from mice for tissue ELISA. RIPA lysis buffer (Solarbio, Beijing, China) was prepared and supplemented with 1% PMSF (TargetMol, MA, USA) and 1% phosphatase inhibitors (TargetMol, MA, USA). Using a glass homogenizer, skin specimens were homogenized at a ratio of 0.1 g of ground tissue per 1 mL of lysis buffer. The homogenates were transferred to 1.5 mL tubes and centrifuged at 10,000 rpm for 10 min at 4 °C, and the supernatant was stored at 80 °C until analyzed. Prior to testing, the supernatant protein concentration was quantified by a bicinchoninic acid (BCA) assay, using BCA protein assay kits (Seven Biotech, Beijing, China). The supernatant protein concentration was then normalized to a standard value. TNF-α, IL-6, and IL-1β protein levels were determined using ELISA kits (Ruixinbio, Quanzhou, China).

Statistical analysis

At least three independent experiments were performed. Results are presented as mean ± standard error of the mean (SEM). Statistical analysis was performed by Student's t-test and Mann-Whitney U test using IBM SPSS Statistics 25 (IBM SPSS, Armonk, NY, USA). $P<0.05$ was considered statistically significant. Results are shown as mean ± SEM. Graphs were generated using GraphPad Prism version 9.5.

Results

In this study, the MAPs were discovered in our previous works, published as patents. They can be found on the WIPO website under grant number CN112961210 and CN112851799. The information on the three MAPs is listed in the supplementary materials Table S1.

Antibacterial activity of the MAPs in vitro and in vivo

It was proved the antibacterial activity in vitro of hLFT-68, hLFT-309, and bLGB-111 against *S. aureus* and *E. coli*. The results of MIC and IC_{50} are listed in Table 1. In all of them, bLGB-111 had the best antibacterial function against *S. aureus* and *E. coli*. The in vivo assessment of antimicrobial efficacy was performed using a 3-day infected full-thickness wound model, as described in Sect. 2.6, *In vivo study of antimicrobial efficacy.* The colony number of wound bacteria cultures in the control, hLFT-68, hLFT-309, and VAN groups on the third day was respectively 3227, 1065, 1193, and 2 on average (Fig. 1). It was verified that the MAPs possess the ability to

MAP	MIC (mg/mL)		IC_{50} (mg/mL)	
	S. aureus	*E. coli*	*S. aureus*	*E. coli*
hLFT-68	12.8	12.8	8.44	6.79
hLFT-309	51.2	25.6	28.23	14.71
bLGB-111	12.8	12.8	3.73	5.90

Table 1. MIC and IC_{50} of the MAPs against *S. aureus* and *E. coli*.

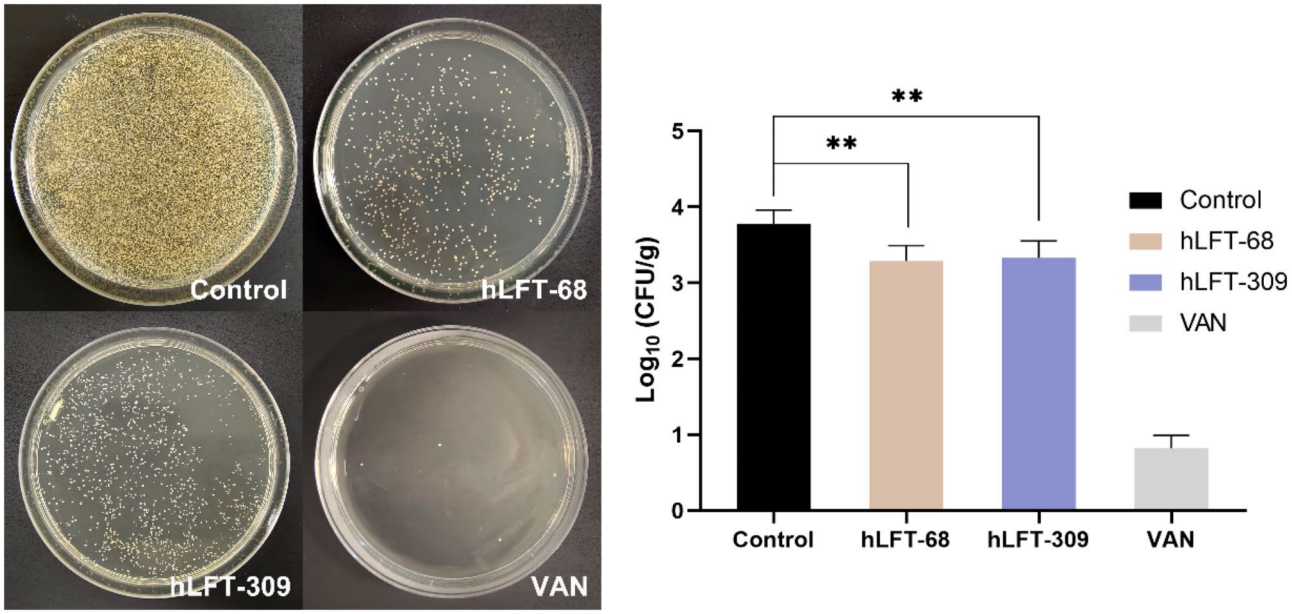

Fig. 1. The MAPs inhibited bacteria in vivo. The left images are representative pictures of bacteria cultured from *S. aureus*-infected wounds with different treatments (control, hLFT-68, hLFT-309, and VAN) on day 3. The colony number on the TSB agar medium was also counted by the Image-Pro Plus 6.0 program. $^{**}P < 0.01$, $N = 3$ per group.

inhibit bacterial proliferation in wound beds, although the reduction in bacterial colonies in MAP-treated mice (approximately 1-log decrease compared to control) was lower than the more than 3-log reduction observed in VAN-treated mice. This may be attributed to the administration method of the MAPs and their instability in vivo. In our future studies, we plan to explore strategies such as increasing the concentration, enhancing the dosing frequency, and modifying the formulation or delivery system to improve the antimicrobial efficacy of the MAPs in vivo. Additionally, in our preliminary experiments, bLGB-111 exhibited relatively weaker activity in promoting in vitro wound healing compared to hLFT-68 and hLFT-309. So hLFT-68 and hLFT-309 were selected as the primary subjects for further investigation in this study. Because bacterial colonization on the surface of the skin is clearly exposed to higher concentrations of the drug compared to the concentrations that reach the skin cells, lower concentrations were used in following cell experiments.

Anti-inflammatory activity of the MAPs in vitro

It was found that LPS-induced production of IL-1β, IL-6, and TNF-α in RAW264.7 cells was decreased by the treatment of various concentrations of hLFT-68 and hLFT-309 in Fig. 2. The hLFT-68 reduced IL-1β secretion concentrations by 1.3 ng/mL at 1 μg/mL, 2.8 ng/mL at 10 μg/mL, and 1.5 ng/mL at both 50 and 100 μg/mL respectively. The hLFT-68 reduced TNF-α secretion concentrations by 9.8–11.2 ng/mL at 10–500 μg/mL, whereas IL-6 showed little decrease. Through the treatment of hLFT-309, IL-1β secretion concentrations declined by 2.0 ng/mL at 1 μg/mL and 2.5 ng/mL at both 10 and 50 μg/mL, IL-6 secretion concentrations was reduced by 6.0-6.9 ng/mL at 1–100 μg/mL and 9.1 ng/mL at 500 μg/mL, and TNF-α secretion concentrations declined by 16.0-12.1 ng/mL at 1–500 μg/mL respectively. The results demonstrated that MAPs exert a cellular anti-inflammatory effect. Notably, this anti-inflammatory activity was not concentration-dependent. The dose difference facilitated the identification of an effective concentration range for their anti-inflammatory properties.

Skin cell proliferative activity of the MAPs in vitro

Fibroblasts and keratinocytes are the cells that are crucial for dermal tissue repair in wound healing during the proliferation phase[3]. HSF and HaCaT cells were chosen as the test cells of fibroblast and keratinocyte respectively. To accurately determine the EC_{50} values, we adopted the different dose ranges. At concentrations of

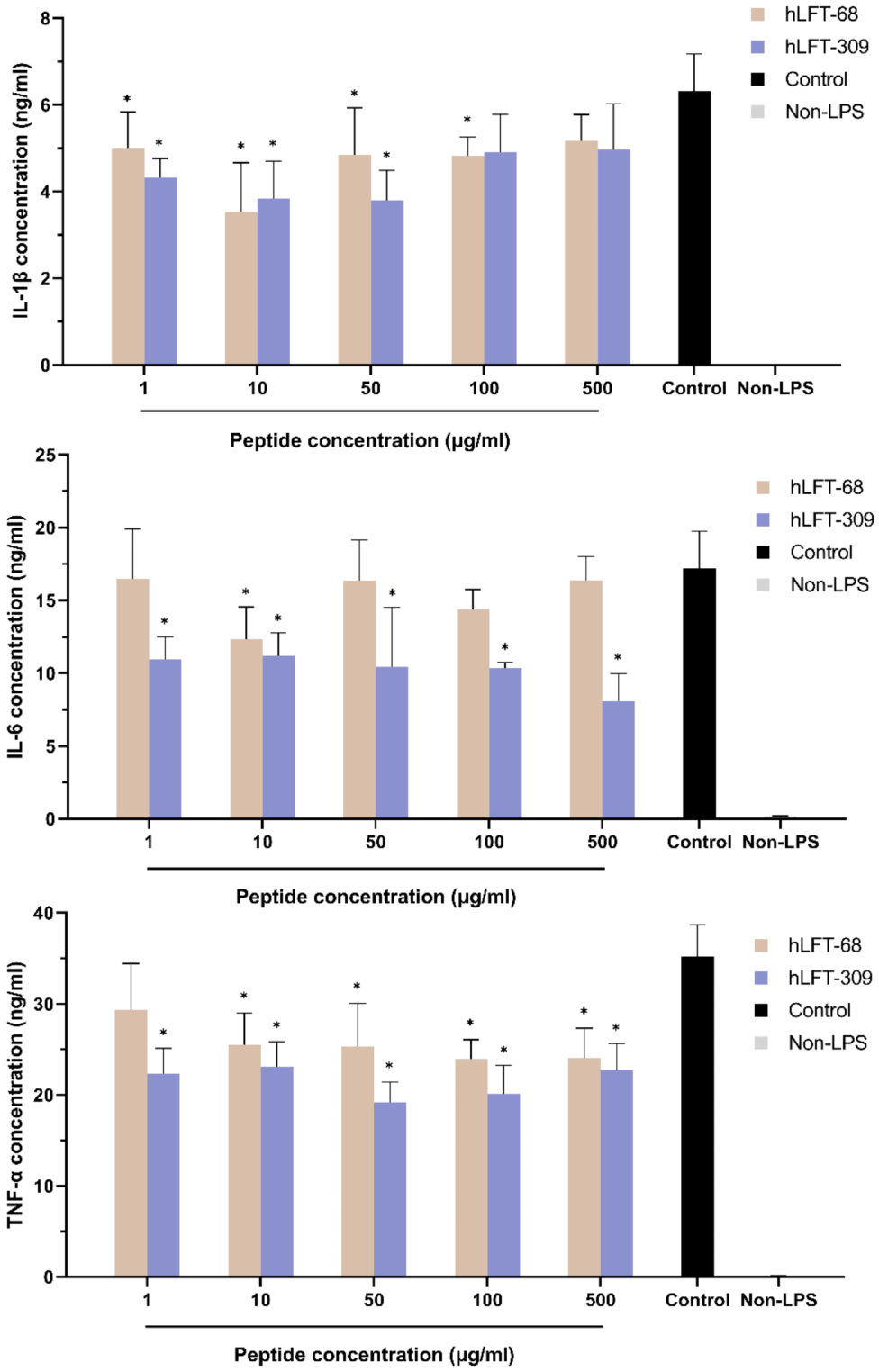

Fig. 2. The MAPs reduced the secretion of inflammatory factors from LPS-stimulated RAW264.7 cells. The non-LPS group was used to detect whether LPS successfully induced RAW264.7 cells to secrete inflammatory factors. **(A)** After treatment with hLFT-68 (1, 10, 50, 100, and 500 μg/mL), hLFT-309 (1, 10, 50, 100, and 500 μg/mL), or PBS (control), the LPS-stimulated RAW264.7 cell supernatant of IL-1β content was tested by ELISA. *$P<0.05$ vs. control, $N=5$ per group. **(B)** After treatment with hLFT-68 (1, 10, 50, 100, and 500 μg/mL), hLFT-309 (1, 10, 50, 100, and 500 μg/mL), or PBS (control), the LPS-stimulated RAW264.7 cell supernatant of IL-6 content was tested by ELISA. *$P<0.05$ vs. control, $N=5$ per group. **(C)** After treatment with hLFT-68 (1, 10, 50, 100, and 500 μg/mL), hLFT-309 (1, 10, 50, 100, and 500 μg/mL), or PBS (control), the LPS-stimulated RAW264.7 cell supernatant of TNF-α content was tested by ELISA. *$P<0.05$ vs. control, $N=5$ per group.

2, 10, 20, and 50 μg/mL, hLFT-68 statistically significantly increased HSF proliferation by 14, 20, 21, and 22%, while hLFT-309 at 10, 20, and 50 μg/mL increased by about 14%, and bLGB-111 at 20 and 50 μg/mL increased by about 4%, respectively (Fig. 3A). The EC_{50} values (μg/mL) of MAPs-treated HSF proliferation were calculated, respectively 62.19 in the hLFT-68 group, 12.55 in the hLFT-309 group, and 62.34 in the bLGB-111 group, aiming to determine the appropriate concentration for subsequent experiments[30]. Through the EC_{50} values, hLFT-309 had the most efficient proliferation.

In the cell proliferation assay of HaCaT cells, hLFT-68 (0.2–500 μg/mL), hLFT-309 (10–500 μg/mL), and bLGB-111 (2–500 μg/mL) had a noteworthy positive effect on cellular proliferative activity (Fig. 3B). Meanwhile, hLFT-68 increased HaCaT cell proliferation by up to 36% at 500 μg/mL, hLFT-309 increased by up to 71% at 50 μg/mL, and bLGB-111 increased by up to 40% at 500 μg/mL. The pro-proliferative abilities of hLFT-68 and

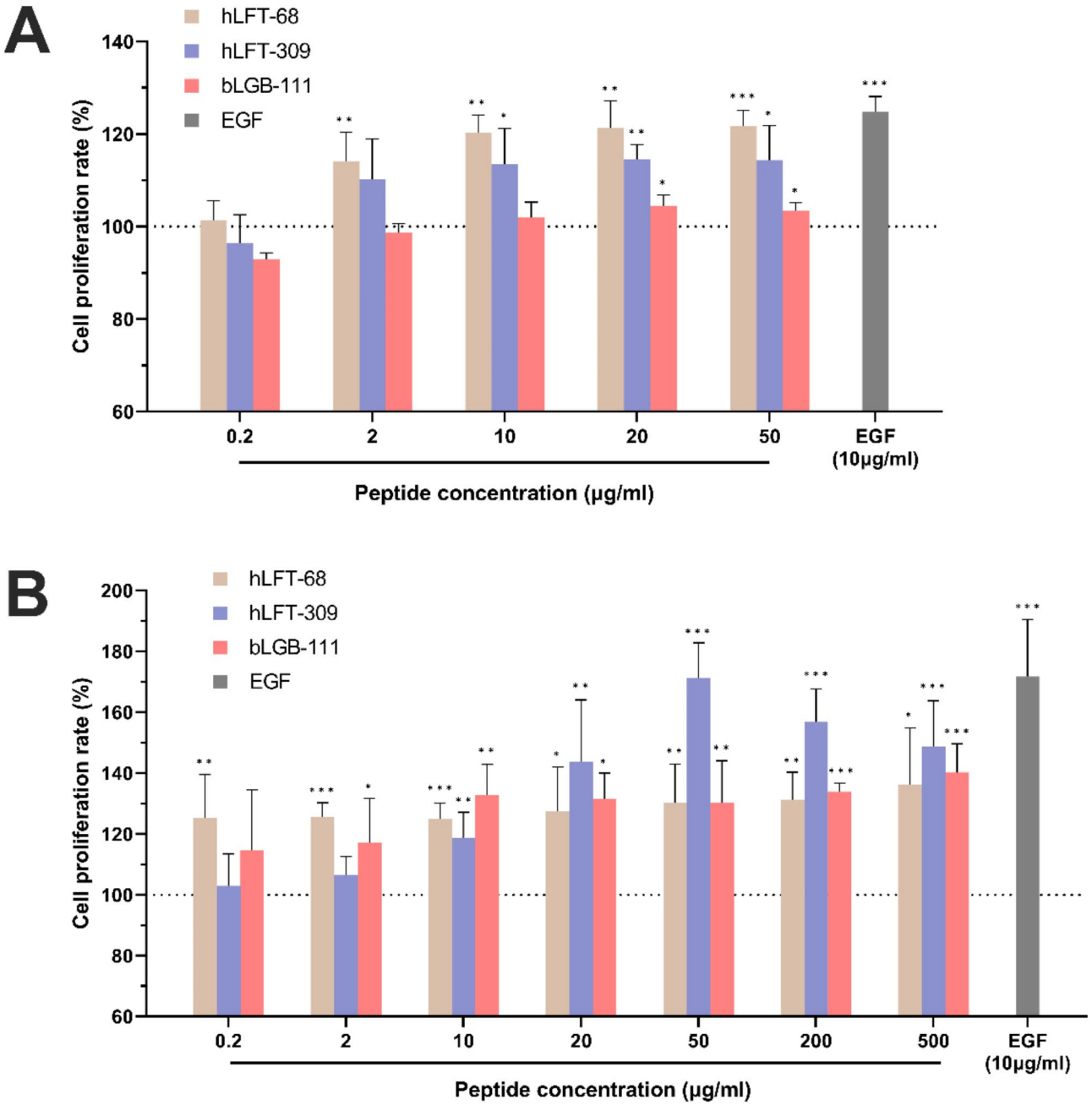

Fig. 3. The MAPs promoted HSF and HaCaT cell proliferation. **(A)** Effect of the MAPs on HSF proliferation. HSFs were treated with hLFT-68 (0.2, 2, 10, 20, and 50 μg/mL), hLFT-309 (0.2, 2, 10, 20, and 50 μg/mL), or EGF (10 μg/mL, positive control). $^{*}P<0.05$ vs. 100%, $^{**}P<0.01$ vs. 100%, $^{***}P<0.001$ vs. 100%, $N=5$ per group. **(B)** Effect of the MAPs on HaCaT cell proliferation. HaCaT cells were treated with hLFT-68 (0.2, 2, 10, 20, 50, 200, and 500 μg/mL), hLFT-309 (0.2, 2, 10, 50, 200, and 500 μg/mL), or EGF (10 μg/mL, positive control). $^{*}P<0.05$ vs. 100%, $^{**}P<0.01$ vs. 100%, $^{***}P<0.001$ vs. 100%, $N=5$ per group.

hLFT-309 were both approximately better than those of bLGB-111 in general, so hLFT-68 and hLFT-309 were selected as the main experimental subjects in this study.

Acceleration of wound healing by the MAPs in vivo

In a 12-day *S. aureus*-infected full-thickness wound mouse model, the back wounds were treated with 50 μL of PBS as a control, hLFT-68 at 0.5 mg/mL, hLFT-309 at 0.5 mg/mL, and EGF at 5000 IU/mL as a positive control twice a day. The chart in Fig. 4A showed that hLFT-68 and hLFT-309 accelerated the recovery of wounds, particularly most quickly on days 5 and 7. On day 5, the wound repair rates of the hLFT-68 and hLFT-309 groups were, respectively, 65% and 75%, which were 17% and 35% higher than the one in the control group. The wound repair rates of the control and EGF groups were both about 55%. It is interesting to point out that the infection prevented EGF from promoting wound healing during the early phases, but the MAPs did not. And the pro-inflammatory effect of EGF resulted in a decrease in wound repair rate on day 3. The pictures in Fig. 4B showed that the wound area in the hLFT-68 and hLFT-309 groups shrank faster than that in other groups. Besides, EGF stimulated the formation of hair follicles, whereas the MAPs had a minimal effect.

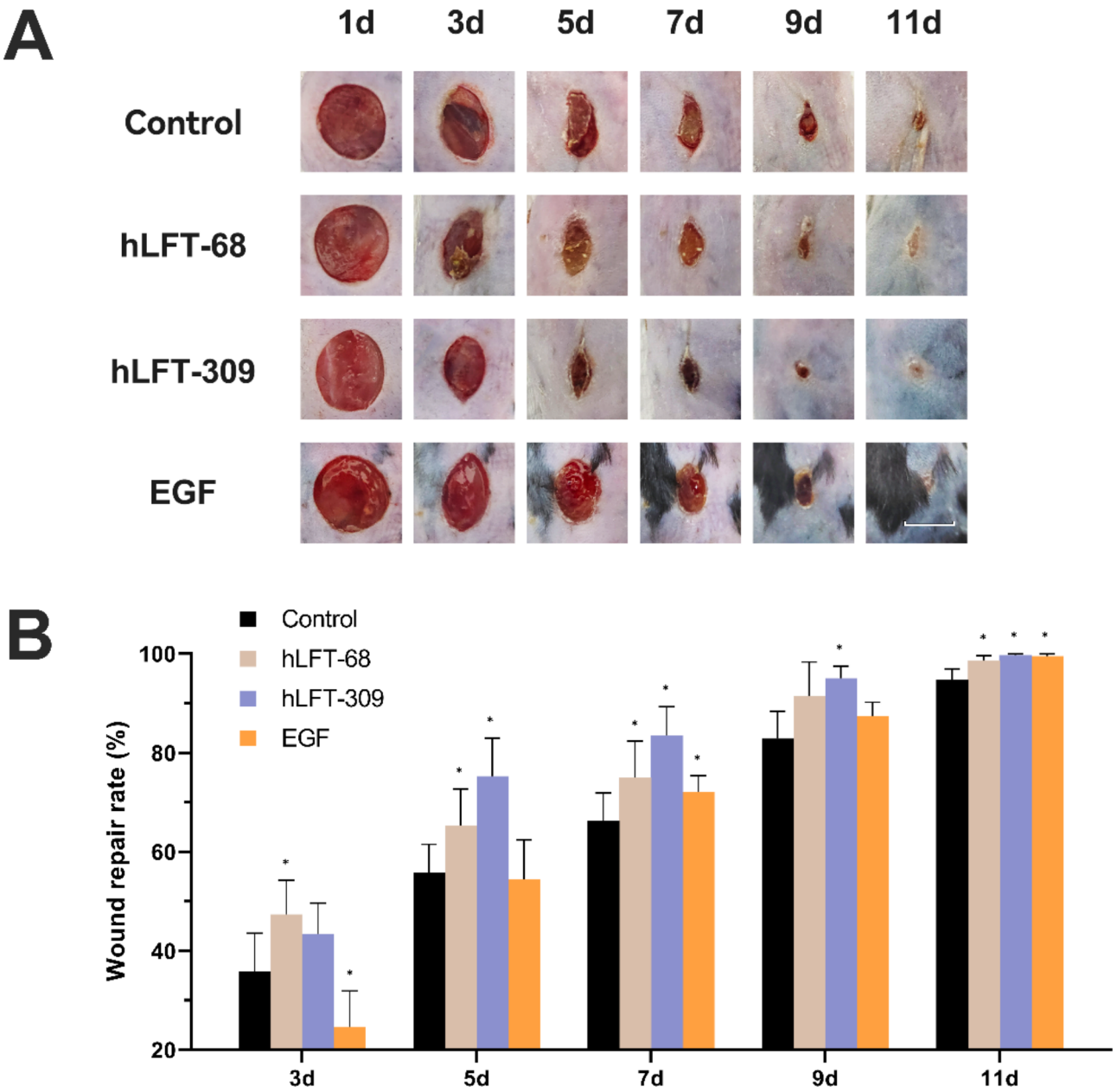

Fig. 4. The MAPs enhanced wound healing in vivo. **(A)** Representative pictures of *S. aureus*-infected wounds with different treatments (Control, hLFT-68, hLFT-309, and EGF) on different days (scale bar = 0.5 cm). **(B)** The percentage of the wound repair areas for each group on days 3, 5, 7, 9, and 11. $^{*}P < 0.05$ vs. control, $N = 10$ per group.

To eliminate the potential confounding effect of infection on wound healing, we further investigated the pro-healing effects of MAPs in a pilot experiment using an infection-free model, as detailed in the Supplementary Material Fig. S1. The hLFT-309 enhanced wound healing in a mouse wound model without infection (*$P < 0.05$, $N = 3$ per group). Other experimental conditions were consistent with an infected full-thickness wound mouse model in the main text.

The MAPs reduced wound inflammation by declining inflammatory factor secretion

It was demonstrated that the MAPs had anti-inflammatory properties in vitro, and our findings applied to the mouse model as well. Through the inflammation score, it was observed that the MAPs were effective in reducing skin redness and the amount of exudate, as well as preventing purulent and bloody secretions from the wound. By day 3, the inflammation score in the hLFT-68 and hLFT-309 groups had dropped to about 8 points and remained there for 6 days, which was 25% lower than the control group. By day 9, the hLFT-68 and hLFT-309 groups' scores dropped to about 5 points. However, the inflammation score in the control and EGF groups decreased to 8 points on days 9 and 5, respectively (Fig. 5A). With the treatment of the MAPs and compared to the control group, the concentration of inflammatory factors IL-1β and TNF-α in cutaneous wounds decreased, but IL-6 had little statistically significant reduction. On day 8, inflammatory factor secretion was generally lessened to about normal or day 12 levels (Fig. 5B,C).

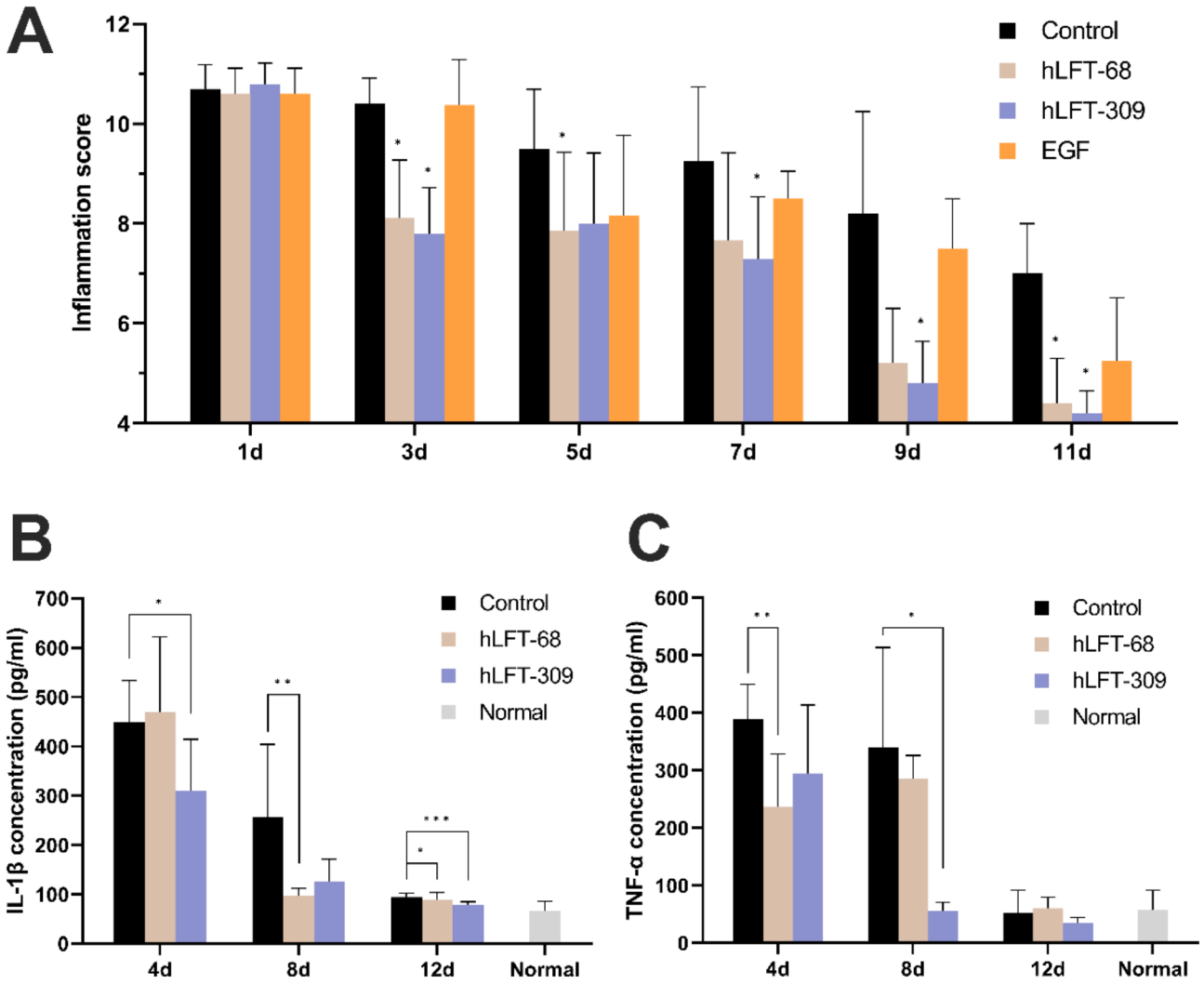

Fig. 5. In vivo, wound inflammation was decreased by the MAPs. **(A)** The inflammation score of *S. aureus*-infected wounds with different treatments (Control, hLFT-68, hLFT-309, and EGF) on days 1, 3, 5, 7, 9, and 11. *$P < 0.05$ vs. control, $N = 10$ per group. **(B)** IL-1β concentration of skin tissue in the wound site for each group on days 4, 8, and 12. The normal group means skin tissue comes from normal skin without a wound. *$P < 0.05$, **$P < 0.01$, ***$P < 0.001$, $N = 3$ per group. **(C)** TNF-α concentration of skin tissue in the wound site for each group on days 4, 8, and 12. The normal group means skin tissue comes from normal skin without a wound. *$P < 0.05$, **$P < 0.01$, $N = 3$ per group.

The MAPs enhanced collagen synthesis and angiogenesis in skin wounds

Masson staining analysis was used to evaluate collagen deposition, homogenous collagen distribution, and evident skin appendage regeneration. The results are shown in Fig. 6A. The hLFT-68 and hLFT-309 groups showed enhanced collagen deposition, homogenous collagen distribution, and evident skin appendage regeneration. In contrast, fewer collagen fiber deposits and an uneven collagen fiber arrangement were seen in the control group, and there was negligible cutaneous appendage regeneration (Fig. 6A-1). The collagen volume fraction is the proportion of collagen area in the total dermal tissue area. The collagen volume fraction in the MAP-treated groups was significantly higher than that in the control group and decreased with the development of the wound. On day 4, the collagen volume fractions had the largest increase, improved by 30% in the hLFT-68 and hLFT-309 groups, and then gradually decayed (Fig. 6A-2). In the cutaneous collagen fiber production of the hLFT-68 and hLFT-309 groups, there was a substantial drop in collagen type III and an elevated level in collagen type I. Consequently, it caused a sharp increase in collagen types I and III ratios when compared to the control group (Fig. 6B). Collagen I is a stiff fibrillar protein that provides tensile strength, mostly synthesized in the middle and late stages of wound healing. It is a marker of collagen maturation. On the contrary, collagen III forms an elastic network that stores kinetic energy as an elastic rebound. Hence, an elevation in the collagen types I and III ratios could be considered a symbol of a healed and matured wound[34,35]. According to an analysis of immunohistochemistry for the vascular endothelial cell marker CD31, the dermal tissue of MAP-treated groups showed greater CD31-specific staining in the wound area than the control group. It could be concluded that the MAPs effectively induced the upregulation of tissue CD31 expression and a concurrent increase in the number of wound blood vessels. On day 12, the hLFT-68 group exhibited the most significant increase in CD31 expression, with an improvement of 160%, while the hLFT-309 group showed a 75% increase. It was determined that the MAP-treated wound area had an upsurge in neovascularization over time (Fig. 6C).

Discussion

According to the results about the mechanism and actions of the MAPs on cutaneous wound healing, how the MAPs affect the progression of the wound healing phases should be looked into, which works like Fig. 7. The antimicrobial and anti-inflammatory properties of the MAPs can suppress bacteria-induced inflammation and the inflammatory secretion of macrophages during the inflammation phase of wound healing, or even at earlier stages. This may facilitate the rapid transition of the wound from the inflammation phase to the proliferation phase. Furthermore, the cellular proliferative effects of the MAPs can promote the proliferation of fibroblasts and keratinocytes during the proliferation phase, thereby accelerating collagen synthesis and ECM deposition in the wound bed.

Antibacterial function plays a central role in the whole wound healing phase and protects from infection. Via the value of MIC and IC50 in Table 1, it was found that hLFT-68, hLFT-309, and bLGB-111 have a modest antimicrobial potency (1–100 mg/mL), compared to other antimicrobial peptides promoting wound healing (1–1000 μg/mL)[26,27,36–38]. And the antibacterial potency is consistent with recent studies on food-derived antimicrobial peptides[39]. Meanwhile, the *S. aureus*-infected full-thickness wound mouse models were treated with the MAPs, and these drugs effectively inhibited the colony expansion of *S. aureus* on the surface of wounds. The further antibacterial mechanisms of the MAPs, such as the carpet model, barrel-stave model, toroidal model, and others, necessitate a deeper investigation[40,41]. Recent studies indicate that the antibacterial effects of antimicrobial peptides primarily stem from their ability to disrupt microbial cell membranes or regulate bacterial genomes[42]. We hypothesize that the mechanisms underlying the activity of our antimicrobial peptides are predominantly attributable to these two processes.

During the inflammation phase, a wide range of inflammatory factors have received special attention for a long time due to their pro-inflammatory effect on wound healing, including IL-1β, IL-6, and TNF-α. Many studies support that reducing their expression and secretion helps to lower cutaneous inflammation and accelerate wound healing[5,16,43,44]. Macrophages play a role in controlling infections and developing inflammation. They are the key inflammatory cells that release these cytokines. In this study, LPS-stimulated RAW264.7 cells were chosen as model cells of macrophages[45–47]. Employing LPS-treated RAW264.7 models, it was discovered that the MAPs decreased TNF-α, IL-6, and IL-1β released by macrophages. Meanwhile, the mouse model also corroborated this phenomenon, and the MAPs reduced inflammation in infected wounds on the back of mice. Antimicrobial peptides have anti-inflammatory mechanisms that inhibit the generation of transcription factors, regulate inflammation-related signaling pathways, or decrease the ability of inflammatory inducers to bind to their sensors[48]. Because of their inhibitory role in cellular mechanisms, we suppose the MAPs can downregulate inflammation-related signaling pathways. LPS can combine with the Toll-like receptor (TLR)4 to activate the TLR pathway, downstream nuclear factor-kappa B (NF-κB), and mitogen-activated protein kinase (MAPK) pathway[49]. NF-κB pathway controls the expression of TNF-α, IL-1β, IL-6, and inflammatory chemokines. NF-κB plays an essential role in regulating and expressing various inflammatory response-related genes[50]. The MAPs may inhibit TLR4-mediated NF-κB and MAPK pathways, resulting in significant anti-inflammatory effects, like the antimicrobial peptides OIR3[51], SET-M33, and SET-M33D[47,52].

During the proliferation phase, fibroblasts replace the initial fibrin clot with granulation tissue, keratinocytes proliferate and migrate to cover the wound gap and blood vessels reconstruct via the angiogenesis of vascular endothelial cells[2]. In the HaCaT and HSF cells proliferative models, it was found that the MAPs enhance the cell proliferation rate. Additionally, synthesis, deposition, and maturation of the collagen were encouraged by the treatment of the MAPs in vivo. It is proved that the MAPs enhanced the proliferation of fibroblasts and keratinocytes, improved collagen production from fibroblasts and keratinocytes, accelerated the deposition of ECM, led to re-epithelialization and granulation tissue formation, and finally promoted angiogenesis and wound repair. It is reported that different wound healing peptides enhance re-epithelialization via activating receptor-signaling mechanisms responsible for cell migration and proliferation, such as phospholipase C-beta

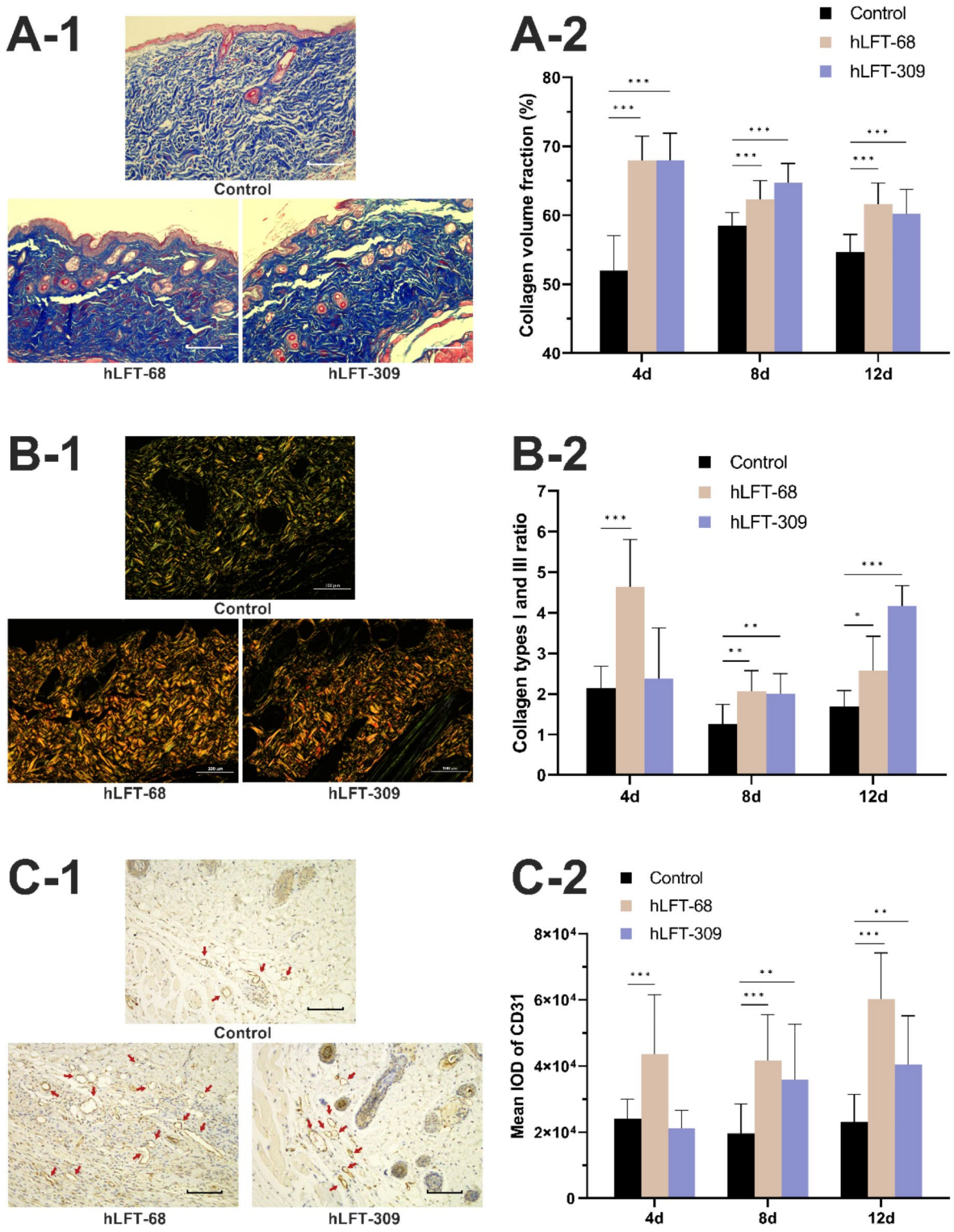

Fig. 6. The MAPs increased angiogenesis and accelerated the synthesis and maturation of collagen. **(A-1)** Masson staining section images of *S. aureus*-infected wounds with different treatments (Control, hLFT-68, and hLFT-309) on day 4. Blue staining represents collagen fibers. (scale bar = 100 μm) **(A-2)** Collagen volume fraction for each group on days 4, 8, and 12. ***$P < 0.001$, $N = 3$ per group. **(B-1)** Under polarized light microscopy, Sirius red staining section images of skin tissue in the wound site for each group on day 12. The orange and yellow staining indicate collagen type I, while the green staining represents collagen type III. (scale bar = 100 μm) **(B-2)** Collagen types I and III ratio of skin tissue in the wound site for each group on days 4, 8, and 12. *$P < 0.05$, **$P < 0.01$, ***$P < 0.001$, $N = 3$ per group. **(C-1)** CD31 IHC staining section images of skin tissue in the wound site for each group on day 12. Brown staining represents CD31 expression. Red arrows refer to micro and small vessels. (scale bar = 100μm) **(C-2)** Their mean IOD of skin tissue in the wound site for each group on days 4, 8, and 12. **$P < 0.01$, ***$P < 0.001$, $N = 3$ per group.

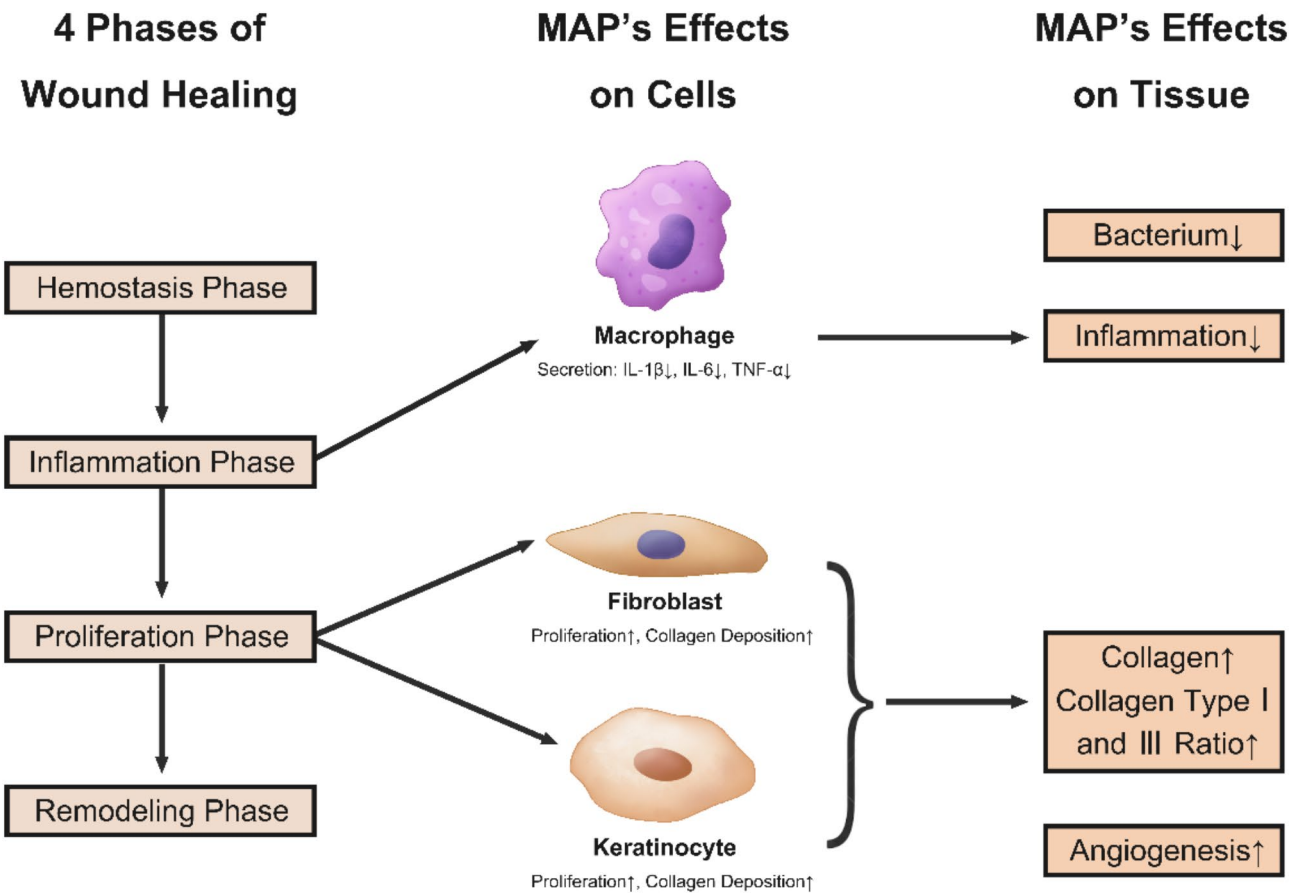

Fig. 7. Cellular mechanisms of the MAPs' effect on wound healing. The MAPs can lessen wound inflammation by causing a reduction in the inflammatory factors secreted by macrophages during the inflammation phase. To improve the synthesis and deposition of collagen, the MAPs can stimulate the proliferation of fibroblasts and keratinocytes during the proliferation phase.

(PLC-β), EGF receptor (EGFR), and phosphoinositide-3 kinase (PI3K)/Akt/mechanistic target of rapamycin (mTOR) pathway[4]. Finally, the optimal concentration for each above function may differ, consistent with other studies demonstrating varying concentration-response relationships for antimicrobial peptides[53,54]. Our future investigations will focus on maximizing the multifunctional effects of MAPs, with subsequent studies on delivery systems aimed at optimizing the most effective concentrations for each specific activity.

In the preliminary experiments, MAP treatment did not affect the HSF cell migration and the expression of proteins EGF, fibroblast growth factor (FGF)-1, transforming growth factor (TGF)-β1, and alpha-smooth muscle actin (α-SMA). Human antimicrobial peptides hBD-2 and hBD-3, which are highly expressed by keratinocytes at wound sites, enhance cytokine secretion, cell migration, and proliferation, through the phosphorylation of STAT and the EGFR proteins[55,56]. The lack of migrative activity in the HSF cell scratch assay and no significant difference in the expression of proteins EGF and FGF-1 indicated that the MAPs might not act on wounds through EGFR transactivation and the ERK1/2 signaling pathway[57,58]. It is reported that a high concentration of α-SMA is linked to the capacity of myofibroblasts to produce powerful contractile forces and focal adhesions, and increased TGF-β expression accelerates the differentiation of myofibroblasts[53,59–61]. The absence of a noteworthy variation in the expression of protein TGF-β1 and α-SMA showed MAP treatment might not influence the differentiation from fibroblasts to myofibroblasts during the remodeling phase.

Ultimately, among the three MAPs evaluated, hLFT-309 appears to exhibit the strongest anti-inflammatory and cell proliferative effects, despite demonstrating the lowest antibacterial efficacy. In contrast, bLGB-111 shows the highest antibacterial activity but the weakest wound-healing potential, while hLFT-68 displays moderate performance across all evaluated aspects.

Conclusion and outlook

In this investigation, three novel MAPs, including hLFT-68, hLFT-309, and bLGB-111, were originally found to be capable of promoting wound healing, and some exciting applications for the MAPs in the field of skin regeneration have been discoverd. In vitro studies have shown that the MAPs exhibit antibacterial, anti-inflammatory, and cell proliferative properties. By stimulating skin cell proliferation, collagen synthesis, vascular regeneration, and antibacterial and anti-inflammatory effects, MAPs can aid in healing cutaneous wounds in vivo.

Milk protein may be used as a novel antimicrobial peptide resource in the years ahead. In addition, it is reported that the ideal antimicrobial peptides should possess strong antimicrobial activity, low mammalian toxicity, high environmental stability, low serum binding, easy production, and low cost[62]. Our forthcoming study will endeavor to acquire these MAPs through microbial fermentation of milk proteins, aiming to address challenges related to susceptibility, environment stability, and access difficulty encountered by MAPs. Due to the weak activity of bare MAPs in topical use, it is essential to develop various formulations such as nanoparticles, hydrogels, creams, ointments, and patches to enhance stability, prolong delivery, and maximize efficacy[63]. Simultaneously, their inflammatory and proliferative mechanism will be extensively elucidated in subsequent research. We anticipate seeing the MAPs applied more extensively in clinical wound therapy.

Data availability

All data are included in the manuscript and additional information, and further queries about sharing data can be directed to the corresponding author.

Received: 5 August 2024; Accepted: 14 February 2025
Published online: 22 March 2025

References

1. Bouwstra, J. A. & Honeywell-Nguyen, P. L. Skin structure and mode of action of vesicles. *Adv. Drug Deliv. Rev.* **54**, S41–S55 (2002).
2. Wilkinson, H. N. & Hardman, M. J. Wound healing: cellular mechanisms and pathological outcomes. *Open. Biol.* **10**, 200223 (2020).
3. Rodrigues, M., Kosaric, N., Bonham, C. A. & Gurtner, G. C. Wound healing: a cellular perspective. *Physiol. Rev.* **99**, 1 (2019).
4. Miao, F. et al. Antimicrobial peptides: the promising therapeutics for cutaneous wound healing. *Macromol. Biosci.* **21**, e2100103 (2021).
5. Ito, D. et al. Systemic and topical administration of spermidine accelerates skin wound healing. *Cell. Commun. Signal.* **19**, 36 (2021).
6. Chouhan, D., Dey, N., Bhardwaj, N. & Mandal, B. B. Emerging and innovative approaches for wound healing and skin regeneration: current status and advances. *Biomaterials* **216**, 119267 (2019).
7. Ghoreishi, F. S., Roghanian, R. & Emtiazi, G. Novel chronic wound healing by anti-biofilm peptides and protease. *Adv. Pharm. Bull.* **12**, 424–436 (2022).
8. Powers, J. G., Higham, C., Broussard, K. & Phillips, T. J. Wound healing and treating wounds: chronic wound care and management. *J. Am. Acad. Dermatol.* **74**, 607–625 (2016).
9. Huang, C. et al. Anti-inflammatory hydrogel dressings and skin wound healing. *Clin. Transl. Med.* **12**, e1094 (2022).
10. Kaplani, K. et al. Wound healing related agents: ongoing research and perspectives. *Adv. Drug Deliv. Rev.* **129**, 242–253 (2018).
11. Herman, A. & Herman, A. P. Antimicrobial peptides activity in the skin. *Skin. Res. Technol.* **25**, 111–117 (2019).
12. Mazurkiewicz-Pisarek, A., Baran, J. & Ciach, T. Antimicrobial peptides: challenging journey to the pharmaceutical, biomedical, and cosmeceutical use. *Int. J. Mol. Sci.* **24**, 9031 (2023).
13. Ganz, T. et al. Defensins. Natural peptide antibiotics of human neutrophils. *J. Clin. Investig.* **76**, 1427–1435 (1985).
14. Brogden, K. A. Antimicrobial peptides: pore formers or metabolic inhibitors in bacteria? *Nat. Rev. Microbiol.* **3**, 238–250 (2005).
15. Mangoni, M. L., McDermott, A. M. & Zasloff, M. Antimicrobial peptides and wound healing: biological and therapeutic considerations. *Exp. Dermatol.* **25**, 167–173 (2016).
16. Cao, X. et al. Cathelicidin-OA1, a novel antioxidant peptide identified from an amphibian, accelerates skin wound healing. *Sci. Rep.* **8**, 943 (2018).
17. Kazimierska, K. Kalinowska-Lis, U. Milk proteins—their biological activities and use in cosmetics and dermatology. *Mol. Basel Switz.* **26**, 3253 (2021).
18. Samtiya, M. et al. Health-promoting and therapeutic attributes of milk-derived bioactive peptides. *Nutrients* **14**, 3001 (2022).
19. Gallegos-Alcalá, P. et al. Glycomacropeptide protects against inflammation and oxidative stress, and promotes wound healing in an atopic dermatitis model of human keratinocytes. *Foods Basel Switz.* **12**, 1932 (2023).
20. Kumar, N. et al. Nrf2 dependent antiaging effect of milk-derived bioactive peptide in old fibroblasts. *J. Cell. Biochem.* **120**, 9677–9691 (2019).
21. Singh, A. et al. Milk-derived antimicrobial peptides: overview, applications, and future perspectives. *Probiot. Antimicrob. Proteins* **15**, 44–62 (2023).
22. Huan, Y., Kong, Q., Mou, H. & Yi, H. Antimicrobial peptides: classification, design, application and research progress in multiple fields. *Front. Microbiol.* **11**, 582779 (2020).
23. Khan, M. U., Pirzadeh, M., Förster, C. Y., Shityakov, S. & Shariati, M. A. Role of milk-derived antibacterial peptides in modern food biotechnology: their synthesis, applications and future perspectives. *Biomolecules* **8**, 110 (2018).
24. Mohanty, D. P., Mohapatra, S., Misra, S. & Sahu, P. S. Milk derived bioactive peptides and their impact on human health—A review. *Saudi J. Biol. Sci.* **23**, 577–583 (2016).
25. Hassoun, L. A. & Sivamani, R. K. A systematic review of lactoferrin use in dermatology. *Crit. Rev. Food Sci. Nutr.* **57**, 3632–3639 (2017).
26. Tomioka, H. et al. Novel anti-microbial peptide SR-0379 accelerates wound healing via the PI3 kinase/Akt/mTOR pathway. *PLoS ONE* **9**, e92597 (2014).
27. Chen, S. et al. Caerin 1.1 and 1.9 peptides from Australian tree frog inhibit antibiotic-resistant bacteria growth in a murine skin infection model. *Microbiol. Spectr.* **9**, e0005121 (2021).
28. Hamilton-Miller, J. M. Calculating MIC50. *J. Antimicrob. Chemother.* **27**, 863–864 (1991).
29. Tian, M., Liu, J., Chai, J., Wu, J. & Xu, X. Antimicrobial and anti-inflammatory effects of a novel peptide from the skin of frog *Microhyla pulchra*. *Front. Pharmacol.* **12**, 783108 (2021).
30. Luan, S. et al. A microfabricated 96-well wound-healing assay. *Cytom J. Int. Soc. Anal. Cytol.* **91**, 1192–1199 (2017).
31. Wu, S. Y. & Tsai, W. B. Development of an in situ photo-crosslinking antimicrobial collagen hydrogel for the treatment of infected wounds. *Polymers* **15**, 4701 (2023).
32. Zhao, F. et al. A highly efficacious electrical biofilm treatment system for combating chronic wound bacterial infections. *Adv. Mater. Deerfield Beach Fla.* **35**, e2208069 (2023).
33. Bates-Jensen, B. M., McCreath, H. E., Harputlu, D. & Patlan, A. Reliability of the Bates-Jensen wound assessment tool for pressure injury assessment: the pressure ulcer detection study. *Wound Repair. Regen.* **27**, 386–395 (2019).
34. Sofii, I. & Fauzi, A. R. Comparing the effect of tissue adhesive and suturing material on collagen I/III ratio in abdominal skin wounds: an experimental study. *Ann. Med. Surg.* **85**, 5450–5453 (2023).
35. Singh, D., Rai, V. & Agrawal, D. K. Regulation of collagen I and Collagen III in tissue injury and regeneration. *Cardiol. Cardiovasc. Med.* **7**, 5–16 (2023).

36. Liu, Y., Shen, T., Chen, L., Zhou, J. & Wang, C. Analogs of the cathelicidin-derived antimicrobial peptide PMAP-23 exhibit improved stability and antibacterial activity. *Probiot. Antimicrob. Proteins* **13**, 273–286 (2021).
37. Ramezanzadeh, M. et al. Design and characterization of new antimicrobial peptides derived from aurein 1.2 with enhanced antibacterial activity. *Biochimie* **181**, 42–51 (2021).
38. Vergis, J. et al. Antimicrobial efficacy of indolicidin against multi-drug resistant enteroaggregative *Escherichia coli* in a Galleria mellonella model. *Front. Microbiol.* **10**, 2723 (2019).
39. Wang, X. et al. Isolation, identification and characterization of a novel antimicrobial peptide from *Moringa oleifera* seeds based on affinity adsorption. *Food Chem.* **398**, 133923 (2023).
40. Yang, L., Harroun, T. A., Weiss, T. M., Ding, L. & Huang, H. W. Barrel-stave model or toroidal model? A case study on melittin pores. *Biophys. J.* **81**, 1475–1485 (2001).
41. Pouny, Y., Rapaport, D., Mor, A., Nicolas, P. & Shai, Y. Interaction of antimicrobial dermaseptin and its fluorescently labeled analogues with phospholipid membranes. *Biochemistry* **31**, 12416–12423 (1992).
42. Davoudi, M., Gavlighi, H. A., Javanmardi, F., Benjakul, S. & Nikoo, M. Antimicrobial peptides derived from food byproducts: sources, production, purification, applications, and challenges. *Compr. Rev. Food Sci. Food Saf.* **23**, e13422 (2024).
43. Tu, C. et al. Promoting the healing of infected diabetic wound by an anti-bacterial and nano-enzyme-containing hydrogel with inflammation-suppressing, ROS-scavenging, oxygen and nitric oxide-generating properties. *Biomaterials* **286**, 121597 (2022).
44. Zhou, Y. et al. Human adipose-derived mesenchymal stem cells-derived exosomes encapsulated in pluronic F127 hydrogel promote wound healing and regeneration. *Stem Cell. Res. Ther.* **13**, 407 (2022).
45. Xiao, X. et al. A novel antimicrobial peptide derived from bony fish IFN1 exerts potent antimicrobial and anti-inflammatory activity in mammals. *Microbiol. Spectr.* **10**, e0201321 (2022).
46. Zhuo, H., Zhang, X., Li, M., Zhang, Q. & Wang, Y. Antibacterial and anti-inflammatory properties of a novel antimicrobial peptide derived from LL-37. *Antibiotics* **11**, 754 (2022).
47. Brunetti, J. et al. Antibacterial and anti-inflammatory activity of an antimicrobial peptide synthesized with D amino acids. *Antibiotics* **9**, 840 (2020).
48. Luo, Y. & Song, Y. Mechanism of antimicrobial peptides: Antimicrobial, anti-inflammatory and antibiofilm activities. *Int. J. Mol. Sci.* **22**, 11401 (2021).
49. Płóciennikowska, A., Hromada-Judycka, A., Borzęcka, K. & Kwiatkowska, K. Co-operation of TLR4 and raft proteins in LPS-induced pro-inflammatory signaling. *Cell. Mol. Life Sci.* **72**, 557–581 (2015).
50. Liu, L. et al. Progranulin inhibits LPS-induced macrophage M1 polarization via NF-κB and MAPK pathways. *BMC Immunol.* **21**, 32 (2020).
51. Mookherjee, N. et al. Modulation of the TLR-mediated inflammatory response by the endogenous human host defense peptide LL-37. *J. Immunol.* **176**, 2455–2464 (2006).
52. Brunetti, J. et al. Immunomodulatory and anti-inflammatory activity in vitro and in vivo of a novel antimicrobial candidate. *J. Biol. Chem.* **291**, 25742–25748 (2016).
53. Tang, J. et al. A small peptide with potential ability to promote wound healing. *PLoS ONE* **9**, e92082 (2014).
54. Fu, Y. et al. Amphibian-derived peptide homodimer promotes regeneration of skin wounds. *Biomed. Pharmacother.* **146**, 112539 (2022).
55. Niyonsaba, F. et al. Antimicrobial peptides human beta-defensins stimulate epidermal keratinocyte migration, proliferation and production of proinflammatory cytokines and chemokines. *J. Investig. Dermatol.* **127**, 594–604 (2007).
56. Niyonsaba, F., Ushio, H., Nagaoka, I., Okumura, K. & Ogawa, H. The human beta-defensins (-1, -2, -3, -4) and cathelicidin LL-37 induce IL-18 secretion through p38 and ERK MAPK activation in primary human keratinocytes. *J. Immunol.* **175**, 1776–1784 (2005).
57. Takahashi, M. et al. The antimicrobial peptide human β-defensin-3 accelerates wound healing by promoting angiogenesis, cell migration, and proliferation through the FGFR/JAK2/STAT3 signaling pathway. *Front. Immunol.* **12**, 712781 (2021).
58. Yang, X., Song, Y., Sun, Y., Wang, M. & Xiang, Y. Down-regulation of mir-361-5p promotes the viability, migration and tube formation of endothelial progenitor cells via targeting FGF1. *Biosci. Rep.* **40**, BSR20200557 (2020).
59. Darby, I. A., Laverdet, B., Bonté, F. & Desmoulière, A. Fibroblasts and myofibroblasts in wound healing. *Clin. Cosmet. Investig. Dermatol.* **7**, 301–311 (2014).
60. Luetteke, N. C. et al. TGFα deficiency results in hair follicle and eye abnormalities in targeted and waved-1 mice. *Cell* **73**, 263–278 (1993).
61. Mu, L. et al. A potential wound-healing-promoting peptide from salamander skin. *FASEB J.* **28**, 3919–3929 (2014).
62. Li, J. et al. Membrane active antimicrobial peptides: translating mechanistic insights to design. *Front. Neurosci.* **11**, 73 (2017).
63. Thapa, R. K., Diep, D. B. & Tønnesen, H. H. Topical antimicrobial peptide formulations for wound healing: current developments and future prospects. *Acta Biomater.* **103**, 52–67 (2020).

Acknowledgements

This research was supported by the Dalian Medical University-Dalian Institute of Chemical Physics United Innovation Fund (NO. DMU2&DICP UN202311).

Author contributions

X. Li: writing the manuscript, performing the experiments, methodology, data analysis, figure and table preparations. W. Yu assisted in performing the microbial experiments. W. Zhang assisted in performing the in vivo experiments. Y. Yu and H. Cheng: revising the manuscript. Y. Lin and J. Feng: methodology. M. Zhao and Y. Jin: conceptualization, supervision, and resources. All authors reviewed and approved the manuscript.

Declarations

Competing interests

The authors declare no competing interests.

Ethical approval

Experiments were approved and then performed in compliance with the guidelines of the Dalian Institute of Chemical Physics Science Ethics Committee (ethics approval number DICPEC2326). The study is reported in accordance with ARRIVE guidelines.

Additional information

Supplementary Information The online version contains supplementary material available at https://doi.org/10.1038/s41598-025-90685-x.

Correspondence and requests for materials should be addressed to M.Z. or Y.J.

Reprints and permissions information is available at www.nature.com/reprints.

Publisher's note Springer Nature remains neutral with regard to jurisdictional claims in published maps and institutional affiliations.